



1

Journal of Geophysical Research: Space Physics

RESEARCH ARTICLE

10.1002/2015JA020983

Key Points:

- The leading region of the FTE is on closed magnetic field lines
- Magnetosheath ions penetrate into the FTE through its trailing edge
- Magnetosheath electrons are accelerated on opened and closed field lines.

Correspondence to:

O. Le Contel, olivier.lecontel@lpp.polytechnique.fr

Citation:

Roux, A., P. Robert, D. Fontaine, O. Le Contel, P. Canu, and P. Louarn (2015), What is the nature of magnetosheath FTEs?, *J. Geophys. Res. Space Physics*, *120*, doi:10.1002/2015JA020983.

Received 13 JAN 2015 Accepted 13 MAY 2015 Accepted article online 15 MAY 2015

What is the nature of magnetosheath FTEs?

Alain Roux¹, Patrick Robert¹, Dominique Fontaine¹, Olivier Le Contel¹, Patrick Canu¹, and Philippe Louarn²

¹Laboratoire de Physique des Plasmas, UMR7648, CNRS/Ecole Polytechnique/UPMC/University Paris-Sud/Obs. de Paris, Palaiseau, France, ²Institut de Recherche en Astrophysique et Planétologie, CNRS UMR5277/Université Paul Sabatier, Toulouse, France

Abstract Cluster multipoint measurements are used to study two successive magnetosheath flux transfer events (FTEs). Magnetic field lines in the leading region are found to be closed magnetospheric field lines. For event 1 these field lines are wounded up by a large current structure oriented eastward and moving poleward. Conversely, the trailing region corresponds to opened magnetic field lines. For both events the leading edge of the FTEs is a tangential discontinuity separating the magnetosheath from closed field lines. In the case of event 1 magnetosheath ions are accelerated through the FTE trailing edge via a rotational discontinuity and penetrate on closed field lines through a second discontinuity. Thus, the ion jet is accelerated equatorward of the spacecraft but the backtracking of the discontinuities and the lack of dispersion show that ion acceleration occurs at less than $2 R_F$ from Cluster. On the other hand the extrapolation forward indicates that the FTE bulge steepens as in simulations of Dorelli and Bhattacharjee (2009). Evidence is given for the penetration of magnetosheath ions inside the core of the FTE, on closed field lines. Magnetosheath electrons are accelerated in parallel and antiparallel directions on open and on closed field lines, thus breaking the frozen-in condition. Event 2 is also split in two distinct regions but no evidence is found for accelerated bidirectional magnetosheath electrons. For event 2 the two discontinuities at the trailing region are stacked together when they are crossed by the spacecraft, suggesting that the current splitting is a reconnection signature.

1. Introduction

The identification of the process(es) that transports the magnetosheath plasma across the dayside magnetopause is a critical issue in magnetospheric physics. Here we restrict our attention to studying the nonsteady transport associated with flux transfer events (FTEs). Russell and Elphic [1979] have called FTEs magnetic signatures corresponding to transient exchanges of plasma between the magnetosheath and the magnetosphere. A magnetosheath FTE can be defined as a maximum in the modulus of B, together with a bipolar signature on the normal component, in boundary normal coordinates, and often a depression in the density [Paschmann et al., 1982]. For practical reasons we will call magnetosheath FTEs events observed by spacecraft located in the magnetosheath before and after FTE crossing (see taxonomy defined by Elphic [1995]). Statistics made by Berchem and Russell [1984] show that FTE generally move northward, while observed in Northern Hemisphere, and southward in the southern one. These observations suggest that FTEs are formed at low latitudes and move poleward. FTEs are usually represented as twisted open flux tubes linking the magnetosheath to the magnetosphere. This model implies that FTEs are on open field lines; an important issue for our future discussion. Energetic electrons can be used to test field line connectivity. Øieroset et al. [2011] observed untrapped energetic electrons in the core of a plasmoid. They concluded that these electrons were accelerated while the plasmoid was forming. Yet observations of both trapped and untrapped energetic electrons inside a FTE were published by Robert et al. [2006] and by Pu et al. [2013]. Owen et al. [2001] investigated magnetospheric FTEs; they suggested that trapping of energetic (magnetospheric) electrons can take place on the most recently opened flux tube within the FTE. Large-scale simulations of FTE were published; for example, the works of Raeder [2006] and Fedder et al. [2002] help understand the geometry, the topology, and the conditions for FTE formation. Energetic electrons trapped between two hemispheres were identified in global hybrid simulations by Tan et al. [2011]. Dorelli and Bhattacharjee [2009] have conducted resistive MHD simulations of the formation and topology of FTEs. They conclude that FTEs start as flow vortices that bring together topologically distinct magnetic domains thereby driving magnetic reconnection. This process involves the generation of new magnetic separators; a key issue for the present paper. Data taken by most of Cluster instruments

©2015. American Geophysical Union. All Rights Reserved.

2

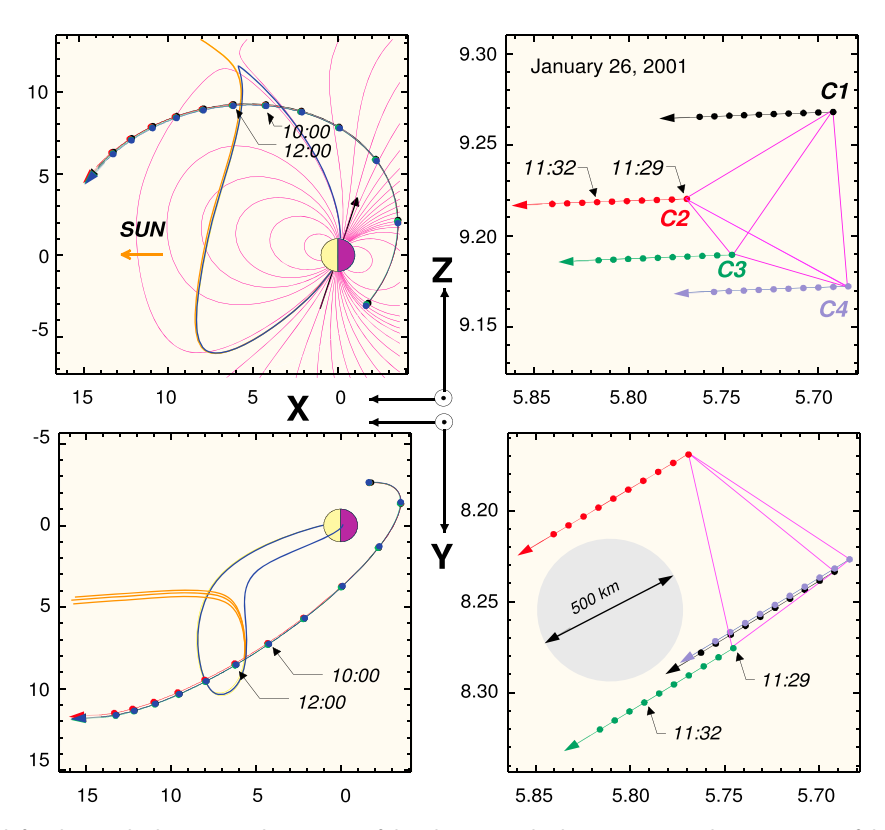


Figure 1. (left column) The location and trajectory of the Cluster tetrahedron in GSE coordinates. A map of the magnetic field configuration, deduced from the Tsyganenko 89 model is superimposed (Figure 1 (top left)); it is plotted in the noon-midnight meridian. Cluster orbital plane is located in the afternoon sector; around 1130 UT, the GSE coordinates (in R_F) are approximately (5.72, 8.25, and 9.22), for the center of mass. (right column) Two projections of the Cluster tetrahedron, also in GSE. As suggested by the figure, the typical distance between the Cluster spacecraft is 500-600 km.

during two consecutive FTEs on 26 January 2001 are analyzed. Previous studies of these FTEs and of the preceding long lasting (almost 2 h) series of fast ion jets and boundary layer and magnetopause crossings were made by Bosqued et al. [2001] and by Phan et al. [2004]. Phan et al. [2004] gave evidence for a series of bulges moving poleward that drive Cluster satellites in and out between the magnetosheath, the boundary layer, and the magnetosphere. They concluded that reconnection was occurring almost continuously (though with temporal modulations) equatorward of Cluster. In section 2 we combine magnetic field data with energetic particle (electrons and ions) signatures in order to determine the topology of magnetic field lines; are they opened or closed? Do they have magnetic footprint(s) on Earth? In section 3 de Hoffman Teller and discontinuity analysis are applied to the abrupt changes observed in plasma parameters within the FTEs, and we try to determine their natures: rotational or tangential discontinuity (RD or TD) or Shock (S). A tentative model of the magnetic structure of the FTEs is discussed in section 4, together with an estimate of how far from Cluster quartet does the acceleration of the ion jet and reconnection take place. In section 5, evidence is given for the penetration of the accelerated ions flow on closed field lines and for the penetration and bidirectional acceleration of magnetosheath electrons on opened and closed field lines. The second event is described in section 6 and compared with event 1. Conclusions are given in section 7.

2. Field Lines Topology

2.1. Context of the Events

Cluster tetrahedron is located in the high-latitude dusk sector, as illustrated by Figure 1. In the whole paper Cluster spacecraft will be referred to as C1 (black), C2 (red), C3 (green), and C4 (blue). They are moving slowly outward. At 1130 UT, the GSE coordinates (in Earth radii hereafter noted R_F) are approximately (5.72, 8.25, 9.22), for the center of mass. Tsyganenko [1987] model is used to plot model field lines, passing by the spacecraft. According to Tsyganenko model, field lines passing by C1, C2, and C3 (yellow) are opened, while the field line passing by C4 (blue) is closed, which indicates that the tetrahedron is close to the nominal magnetopause.

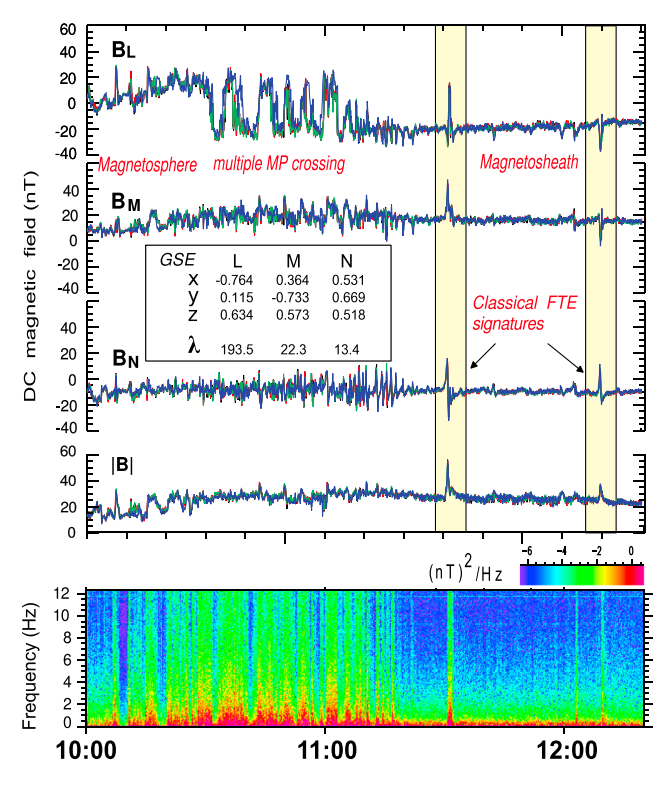


Figure 2. Composite view showing more than 2 h of 4 s resolution wave form data from the fluxgate magnetometer (FGM) and a frequency-time spectrogram from the search coil magnetometer (STAFF). Minimum variance analysis (MVA) has been applied to FGM data; the elements of the rotation matrix are given on the figure, together with the values of λ that characterize the ellipsoid of variance. Yellow bands bracket the two FTEs to be studied.

Two projections of the Cluster tetrahedron, in GSE, are displayed in Figure 1 (right column); they show the typical distance between Cluster spacecraft (500-600 km). Notice that Cluster 4 is somewhat closer from the Earth than its companions.

Figure 2 shows 4 s resolution wave form data from the fluxgate magnetometer (FGM) and a frequency-time spectrogram from the search coil magnetometer (STAFF). For a description of these instruments see *Balogh et al.* [1997] and *Cornilleau-Wehrlin et al.* [1997]. The period covered by Figure 2 was already studied by *Bosqued et al.* [2001] and by *Phan et al.* [2004]. Minimum variance analysis (MVA) has been applied to about 2 h of FGM data; the elements of the rotation matrix are given on the figure, together with the values of λ that characterize the ellipsoid of variance. The three values of λ being quite different, the proper axis of the ellipsoid are well defined, and MVA is accurate. From this MVA, we define the LMN frame for boundary normal coordinates [see *Russell and Elphic*, 1979]. Large-amplitude fluctuations observed in particular on B_L , before 1110 UT, correspond to multiple crossings of the magnetopause. After 1120 UT Cluster spacecraft remain in the magnetosheath, except during short lasting isolated events occurring at ~1131, 1210, and possibly at 1202 UT. In the rest of the paper we focus on the two events observed at ~1131 and ~1210 UT. Unlike magnetopause crossings that occurred around 1100 UT, these events show a large increase in the modulus of B and a bipolar signatures in B_N which are typical of magnetosheath FTE's observed in the Northern Hemisphere.

2.2. Magnetic Structure of the FTE

Full-resolution magnetic field data are plotted in Figures 3a to 3d, for event 1. Boundary normal coordinates, defined in Figure 2, are used. The typical signature of the FTE, with a bimodal signature (\pm) on B_N , is clear. Notice that the modulus of B increases by almost a factor 2 and reaches \sim 55 nT, at \sim 1131:10 UT. This maximum occurs while the leading region of the FTE crosses the spacecraft (region B, \sim 1130:50 to 1131:25). It corresponds to a large decrease in the potential (see Figure 3g) measured by the EFW experiment [Gustafsson et al., 1997]. The potential being a proxy for the density, this period corresponds to a large decrease in the density. The trailing region (region C, \sim 1131:25 to \sim 1131:50) involves two short lasting large rotations in the direction of the magnetic field. In region C the electric potential, and thus the density, is comparable to what

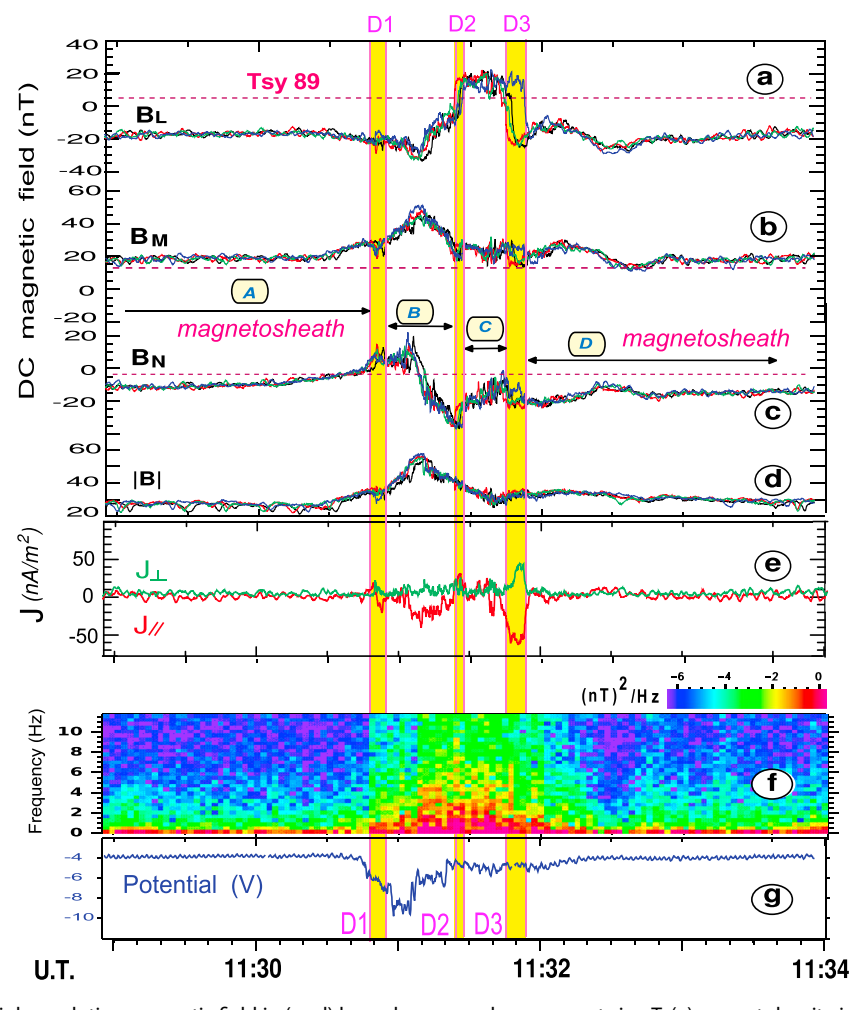


Figure 3. High-resolution magnetic field in (a-d) boundary normal components in nT, (e) current density in nA/m², (f) power spectral density of magnetic fluctuations in $(nT)^2/Hz$, and (g) spacecraft potential in volts, for event 1 and C1. Narrow yellow vertical bands, labeled D1, D2, and D3, delineate sharp transitions between different topological regions labeled A–D.

is found in the magnetosheath, before and after the event (in regions A and D). A dynamical spectrum of magnetic fluctuations is shown in Figure 3f. The level of the fluctuations is strongly enhanced during the FTE. The amplitude (not shown) is $\sim 1-10$ nT/ $\sqrt{\text{Hz}}$. Yellow vertical regions bracketed by pink lines are drawn at the boundaries between different regions; they are labeled D1 (\sim 1130:50), D2 (\sim 1131:25), and D3 (\sim 1131:50). D2 and D3 clearly correspond to sharp discontinuities in the magnetic field. The change in the magnetic field at D1 is smaller, but the density rapidly decreases. Particle data displayed in Figure 4 give evidence for a sharp change at D1 and confirm the existence of a discontinuity. The horizontal violet dashed line corresponds to the magnetic field determined from the *Tsyganenko* [1987] model taken at C4. The large and rapid jumps in B_L at D2 and D3, together with the relatively good agreement between the measured magnetic field and the Tsyganenko field in region C could suggest that the spacecraft was crossing the magnetopause first inward (D2) and later outward (D3). Should this be the case, then one would expect a dip in the density in region C (between D2 and D3). There is indeed a sharp decrease in the potential, and thus in the density, but it occurs in the early part of region B; between D1 and D2. How can this apparent contradiction be explained? The signatures of these two periods on particle data will help resolving this issue, as discussed in sections 2.4 and 2.5.

2.3. Current Density

The distance between Cluster spacecraft is of the order of 500-600 km (see Figure 1), while the typical size of a FTE is of the order of 1 R_E [Saunders et al., 1984]. Thus, the conditions for calculating the current density are generally fulfilled [Dunlop et al., 1990; Robert et al., 1998]. The barycentric method [Chanteur and Harvey,

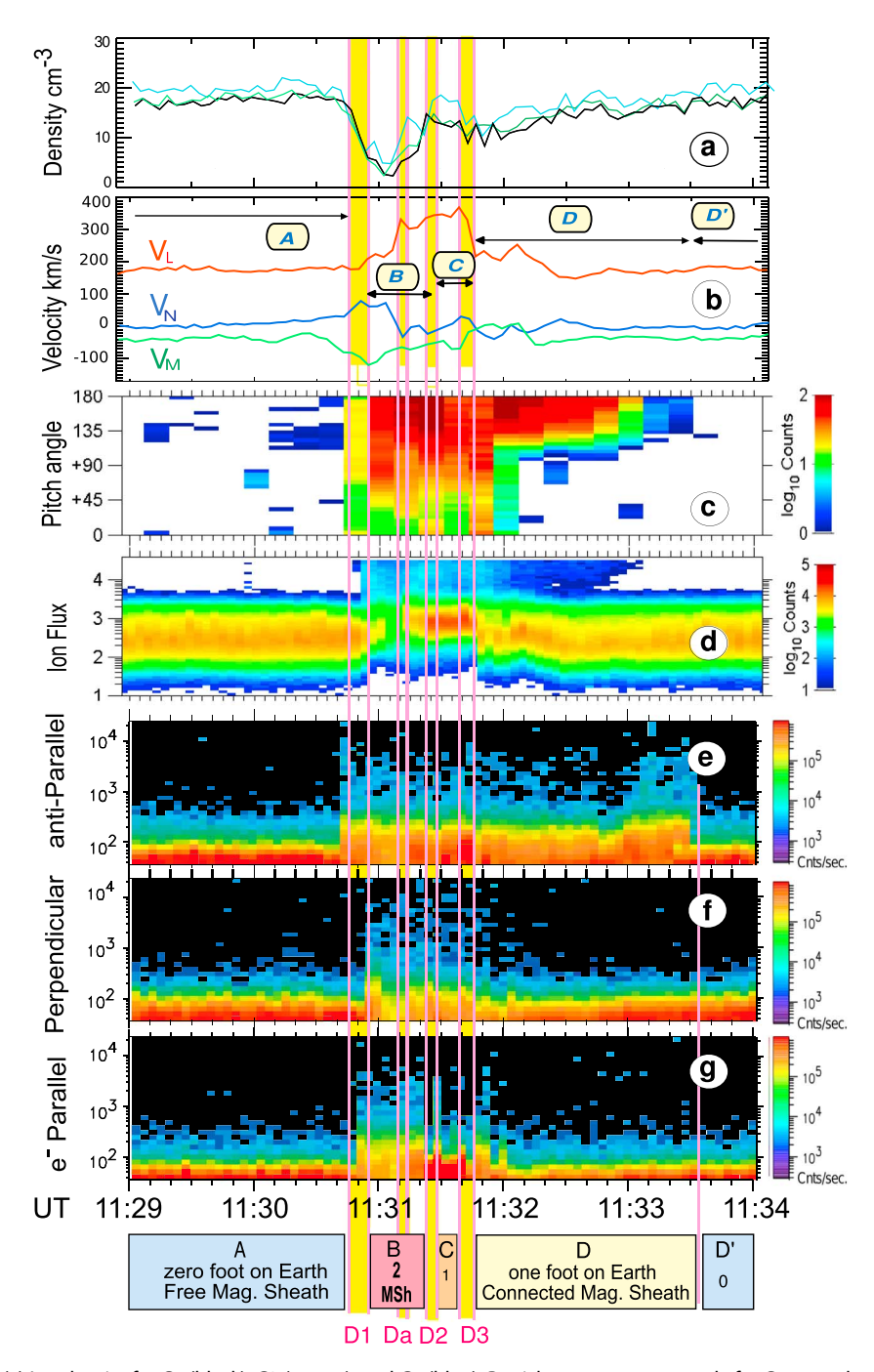


Figure 4. (a) Ion density for C1 (black), C3 (green), and C4 (blue). Particle measurements only for C1, over the same time period as Figure 3. Ion velocity in (b) LMN coordinates, (c) spectrogram of pitch angle distribution of very energetic (> 7 keV) ions, and (d) flux of energetic ions versus energy and time. The electron flux versus energy in the (e) antiparallel, (f) perpendicular, and (g) parallel directions. Notice the sudden increase in the flux of energetic ions and electrons while spacecraft cross D1. Particle data for other satellites are similar. Note also that the discontinuities D1, D2, and D3 found on Figure 3 are also observed in this figure. Yet a fourth discontinuity, Da, is only observable in particle data. Da is located between D1 and D2 (see text).



1998] is used; the resulting current density is plotted in Figure 3e. Around 1131:25 and 1131:50, however, where large short lasting jumps are observed, the linear approximation, used to calculate the current, does not hold. During the leading region of the FTE, where the conditions for estimating $\nabla \times \mathbf{B}$ are satisfied, a relatively large current density is found: $J_{\text{max}} \sim 25 \text{ nA/m}^2$, in region B; this current is essentially antiparallel to B, mostly in the azimuthal direction, toward the evening sector. With such a current magnetic field lines must be strongly twisted. Assuming that the current structure has a radius of $3 \cdot 10^6$ m (35 s times 180 km s⁻¹) and is homogenous over this volume, the corresponding B_L component is ~ -40 nT, opposed to the Tsyganenko magnetic field ($B_L \sim +5$ nT), where the Tsyganenko model is taken as a proxy for the terrestrial magnetic field in the absence of this current. Thus, the magnetic field in region B is dominated by the component associated with the current, and the B_L component is opposed to its expected direction, which explains why B_L is negative on closed field lines and why it can be similar to the magnetic field in the adjacent magnetosheath. In short the leading region of the FTE (region B) corresponds to the core of the flux rope.

2.4. lons

Data from Cluster Ion Spectrometry (CIS) [Rème et al., 1997] are displayed in Figures 4a-4d. Densities measured onboard C1, C3, and C4, displayed in Figure 4a, are consistent with densities estimated from the potential measured by EFW (Figure 3g). Before and after crossing the FTE the density is \sim 15–20 p cm⁻³, suggesting that the spacecraft are located in the magnetosheath. This interpretation is confirmed by data shown in Figure 4d, where large fluxes of low-energy ions, typical of the magnetosheath, are observed together with the absence of energetic ions, before (region A) and well after the FTE (region D'). In the magnetosheath the largest component of the velocity, V₁, is of the order of 180 km s⁻¹ (see Figure 4b) and positive. During the FTE (~1130:50 – 1131:50, corresponding to regions B and C) energetic ions are observed (see Figure 4d) and the flow velocity grows up to twice the magnetosheath value (about 370 km s⁻¹); a classical signature of ion jet. After crossing the FTE the spacecraft returns to the magnetosheath, as testified by the large densities and fluxes, by the low energy of ions and by the flow velocity that returns to about 180 km s⁻¹. Yet energetic ions continue to be observed for about 2 min after FTE crossing (in region D). Figure 4c helps understanding why. During the FTE energetic ions (\sim 7 – 28 keV) extend over most of the pitch angle range. Energetic ions observed after the FTE (in region D), however, only have large pitch angles, close to 180°, which suggests that these ions are escaping along newly opened field lines; a suggestion that will be confirmed by electron observations. Region labeled D' corresponds to the free magnetosheath, without escaping energetic ions. The observation of these energetic ions raises an important question: where do they come from? Are they magnetospheric ions or are they magnetosheath ions accelerated by reconnection, for instance, in the near-equatorial region. At D1 Figure 4d shows that energetic ions above 6 keV undergo little dispersion; at most 4 s delay between 6 and 40 keV. Should energetic ions be accelerated at the equator (at \sim 8 – 10 $R_{\rm F}$) the delay would be \sim 50 to 60 s. The lack of dispersion indicates that the acceleration is local or rather that the spacecraft cross a boundary, in this case the small delay of 4 s is due to finite Larmor radii. This lack of dispersion is also observed on electrons, as seen on Figures 4e-4g. Apart from small time shifts ion data on other spacecraft are very similar.

2.5. Electrons

Figure 4 shows electron fluxes from Plasma Electron and current experiment (PEACE) [Johnstone et al., 1997], in directions antiparallel (Figure 4e), perpendicular (Figure 4f) and parallel (Figure 4g) to B, for C1. As for energetic ions, sharp changes are observed in the flux of energetic electrons while the spacecraft cross D1, D2, and D3. In region A, before crossing D1, there are almost no electron beyond 300 eV, which confirms that region A corresponds to the free magnetosheath. As the spacecraft cross D1 and penetrate into region B, the flux of energetic electrons (1 to 10 keV) sharply increases at all pitch angles (0, 90, and 180° shown here), at about the same time (within one or two spin periods). Given that these energetic electrons would escape from open field lines in a matter of seconds, field lines in region B must be closed to retain energetic electrons at all pitch angles. The local magnetic field being already quite large (~ 50 nT), larger than in the adjacent magnetosheath (< 30 nT), reflection via a magnetic mirror on a newly opened field line is very unlikely. Thus, electrons, observed in region B, should be trapped on closed field lines. Yet there are still two possibilities: energetic electrons can be trapped (i) on field lines that have two magnetic footprints on Earth (a fully Earth connected flux rope) or (ii) on field lines confined inside a plasmoid located outside the magnetopause with no footprint on the Earth. Owen et al. [2001] also observed a possible trapping of energetic magnetospheric electrons on the most recently opened flux tubes at the front of an FTE. A comparison between energetic electron spectra inside the core of the FTE and in the plasmasheet should



help deciding. For instance, at ~1131:19, in the region of closed field lines (region B), the temperature of the energetic component is ~1550 eV. At 1044:22, while the spacecraft were in the plasmasheet the temperature of the energetic component was about the same (\sim 1650 eV) which suggests that trapped energetic electrons come from the magnetosphere. As a further argument we note that more energetic electrons (> 40 keV) are observed by the energetic particle detector RAPID in region B (M. Dunlop, private communication, 2006). Thus, these energetic electrons are likely to be magnetospheric electrons. This result is not surprising because there are several publications demonstrating that FTEs have magnetic signatures on the ground, which strongly suggests that a magnetic connection between at least a part of the FTE and the ground [see, e.g., Marchaudon et al., 2004, and references therein]. In region C energetic electron fluxes are comparable to region B for antiparallel (Figure 4e) and perpendicular fluxes (Figure 4f). Yet there are very few energetic electrons in the parallel direction (Figure 4g); only sporadic bursts lasting less than a spin period are observed, which suggests that field lines in region C are open but continue to be supplied with electrons by reconnecting field line. Thus, the magnetic signature of the FTE involves two distinct regions. Region B (the core of the FTE) corresponds to closed field lines with magnetic footprints on Earth, while region C (the trailing edge of the FTE) corresponds to open field lines. Thus, we observe both trapped and untrapped energetic electrons in different regions of the flux rope. This result confirms preliminary results by Robert et al. [2006] and recent results by Pu et al. [2013]. While Øieroset et al. [2011] observed only untrapped energetic electrons inside the flux rope. Yet the context is quite different; Øieroset et al. [2011] made their observations in the near-equatorial region, ion jets coming from opposite directions. Conversely, the ion jet shown in Figure 4b is observed at relatively high latitude and moves poleward. As for energetic ions, antiparallel energetic electrons continue to be observed in region D, which tells us that the spacecraft remain on open field lines and that energetic electrons (and ions) continue to be supplied by reconnecting magnetospheric field lines, for about 2 min after the crossing of this FTE. Yet in region D the ion flow velocity (Figure 4b) is comparable to magnetosheath values. We label D' (t > 1133:35) the region where the spacecraft return to the free magnetosheath; plasma parameters are about the same as for region A. Based on results presented above, the magnetic topology of the various regions crossed by the spacecraft can be described. Regions A and D' correspond to the free magnetosheath (zero magnetic footprint on Earth). The first period of the FTE (region B) corresponds to a flux rope with closed field lines (two magnetic footprints on Earth) while the second part of the FTE signature (region C) corresponds to opening field lines with one foot on Earth. In region D the spacecraft are still on open field lines but have left the FTE structure. Regions A, B, C, and D are separated by abrupt changes in the parameters, labeled D1, D2, and D3 to be analyzed in section 3. Da corresponds to a decrease in the modulus of the magnetic field (see Figure 3d) associated with an increase in the potential. It coincides with a sharp change in the flux of energetic (keV) ions, as can be seen from Figure 4d.

3. Discontinuity Analysis

3.1. De Hoffmann-Teller Analysis and Walén Test

De Hoffmann-Teller (de HT) analysis and Walén test [Sonnerup et al., 1987] were applied to the ~1131 FTE by Bosqued et al. [2001] and to 1131 and 1210 FTEs by Phan et al. [2004]. Bosqued et al. [2001] obtained similar values for V_{HT} for C1, C3, and C4 (see their Table 1) but found different Walén slopes for the three spacecraft: 0.87 on C1, 0.66 on C3, and 0.44 on C4. Phan et al. [2004] also found very consistent value of the de HT velocity and obtained Walén slopes for C1 close to unity (0.94 and 1) by splitting the ~1131 event in two periods (see their Table 1). The differences between Walén slopes stems from the sensitivity of their estimates to the selected time interval. Here we want to analyze separately the vicinity of each discontinuity within the FTE and are therefore bound to use short time intervals (~ 20 s). The values of the de HT velocity obtained here are given in Table 1 for event 1, spacecraft 1. The de HT velocities are similar to the findings of *Phan et al.* [2004]. $V_{\rm HT}$ reaches ~ 350 km s⁻¹, around Da; much faster than the velocity of the plasma in the free magnetosheath. While the Walén slope around D1 is close to unity it has a large dispersion. Around D3, $V_i - V_{HT} \sim 0.71 V_A$ and the dispersion is small. Around Da and D2 the slopes are far from unity (0.3 and 0.29, respectively). Thus, there is an apparent disagreement between our estimates of the Walén slope and those of *Phan et al.* [2004]. In fact this difference is to be expected because the time intervals that we have selected to analyze separately the four discontinuities inside the FTE turn out to be too short to make a reliable estimate of the Walén slope. In the next subsection an independent evaluation based on a different method will be used.



Table 1	Table 1. For Event 1 ^a					
Line		D1	Da	D2	D3	
1	n _x	0.06	-0.39	- 0.93	-0.83	
2	n_y	0.30	-0.21	0.19	-0.25	
3	n _z	0.95	0.90	-0.30	-0.50	
4	$\Delta \alpha$ (deg)	18	12	18	7	
5	V_D	149	172	225	65	
6	ΔV_D	27	16	56	7	
7	$V ({\rm km \ s^{-1}})$	172	335	329	325	
8	V_X	–129	-292	-263	-235	
9	V_Y	63	73	26	59	
10	V_Z	94	148	196	216	
11	V ⋅ n	100	230	190	73	
12	$V_{\rm HT}$ (km s ⁻¹)	333	347	337	287	
13	$V_{HT,X}$	-260	-287	-259	-217	
14	$V_{HT,Y}$	178	144	82	102	
15	$V_{HT,Z}$	109	131	199	158	
16	V _{HT} ⋅ n	141	198	196	76	
17	$<\theta>$ (deg)	69	15	8.5	16.5	
18	$\Delta heta$	36	12	11.5	12	
19	$< B_n > (nT)$	-0.3	3.5	-3	4	
20	Δho (p cm ⁻³)	-10	-5	small	~0	
21	Summary	$large\theta$	small $ heta$	small $ heta$	small $ heta$	
	large Δho	large Δho	Moderate $\Delta \rho$	small Δho		
	small $\langle B_n \rangle$	$large < B_n >$, $large \Delta \mathbf{V}$	small Δ $f V$	$large < B_n >$		
22	Nature	TD	Undetermined	RD	RD	

^aThe GSE components of the normal vector to each discontinuity are given in the first lines (1–3). Estimates of the standard deviations in the direction of the normal are indicated line 4. Lines 5 and 6 are for the (normal) velocity of the discontinuity and the corresponding standard deviation (in km/s). The ion flow velocities, total, three components, and normal are given lines 7 to 11. The V_{HT}, total, its three components, and normal are given lines 12 to 16. Then θ , the angle between the averaged values of δB_t and δV_t , is shown in line 17 with the estimated standard deviation on θ given in Line 18. The normal components of B, averaged over the four spacecraft, are given line 19. The density jump is displayed line 20. Finally, the main properties are summarized line 21 (ΔV being the jump of the ion velocity vector) and line 22 gives the conclusion in boldface about the nature of each discontinuity.

3.2. Multipoint Analysis

In the present section we propose another type of identification, based upon multipoint analysis tools, to determine the nature of the discontinuities located inside the FTE. Once a time shift is applied, magnetic field components, and flow velocities measured by various spacecraft, have similar time variations. We can therefore assume quasi-stationarity during the crossing of the discontinuities and determine the time shift between each pair of satellites. Knowing the locations of the four spacecraft, and the time of the crossing of each discontinuity by each spacecraft, we calculate the direction of the normal to each discontinuity and its velocity along this normal. Discontinuity analysis was developed by Mottez and Chanteur [1994] and extended by Dunlop and Woodward [1998], Chanteur [1998], Chanteur and Harvey [1998], and Schwartz [1998]. Here we use the method developed by Chanteur [1998] and assume that the four Cluster spacecraft are crossing planar discontinuities.

3.3. Normal Velocities

The velocities of each discontinuity (V_D) is calculated and compared to the projection on its normal of the de HT velocity $(V_{HT,N})$. Table 1 shows that the agreement is quite good; the difference between the two types of estimates is about 10%, which validates the estimates of the normal velocities for each discontinuity.

3.4. Identification of the Discontinuities

The accuracy in the determination of the direction of the normal vectors is estimated from a simulation. Given that the delay Δt between signatures observed by the various spacecraft is the key parameter to determine the direction of the normal vectors, we have randomly added or subtracted ± 0.5 s to the various best estimates of the delays and calculated the corresponding effect on the direction of each normal. The simulation

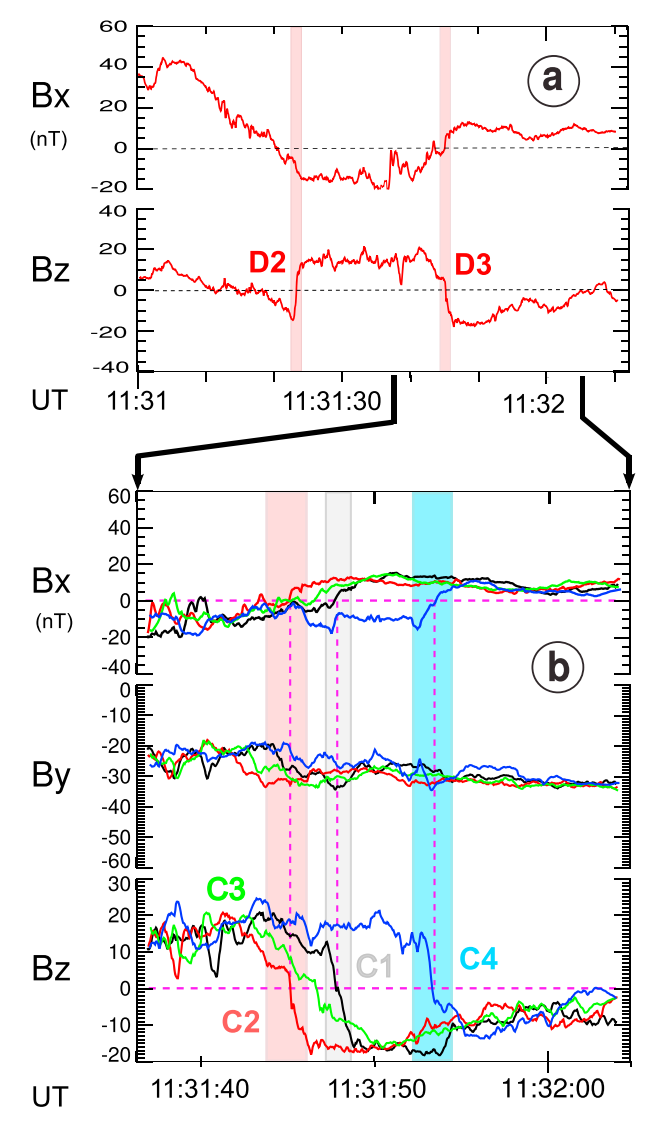


Figure 5. Magnetic field projected on the (XZ)_{qse} plane. (a) Vertical bands point out the rapid reversals in the B_7 component at D2 and D3. (b) A zoom showing the three magnetic field components around D3. All four spacecraft detect similar signatures of thin current sheets at successive times.

involves about 100 combinations of Δt for each discontinuity. Then the standard deviation $\Delta \alpha$ associated with these perturbations is calculated; it gives an estimate of the uncertainty in the determination of the normal. In order to assess the nature of each discontinuity: tangential discontinuity (TD), rotational discontinuity (RD) or shock, three tests are applied. First, we calculate θ , the angle between $\delta \mathbf{B}_{\mathbf{t}}$, the jumps in the magnetic field and δV_t the jump in the ion velocity, projected on the plane of the discontinuity. For a RD or a shock θ should be small [Landau and Lifshitz, 1960]. Second, we estimate $\langle B_n \rangle$, the normal component of the magnetic field, averaged over data from the four spacecraft; it should be very small for a TD. Third, we determine the jump in the density ρ . For a RD the density ρ should be conserved across the discontinuity, while it is likely to undergo a jump for a TD and an increase for a shock. Table 1 gives the outcome of discontinuity analysis, together with estimates of the corresponding uncertainties. The method used to estimate the uncertainties in the determination of θ is described in Appendix A. Table 1 shows that for D1, $\langle B_n \rangle$ is very small, there is a large-density jump and $<\theta>$ is large, larger than the standard deviation taken as an estimate of the error. Hence, D1 is a TD. Da has a relatively large $\langle B_n \rangle$, a large jump of the velocity direction and a small $\theta \sim 14^\circ$; yet it could not be a shock as the normal velocities before and after the discontinuity are about the same magnitude

9

but in the opposite direction and diverging from the discontinuity. Furthermore, as the density and the magnetic field are different for the two regions, mass, and magnetic field fluxes would not be conserved as needed for shock properties. The inconsistency with regard to the conservation laws suggests that the assumption of a planar discontinuity is very likely not relevant. Indeed, Da being located in the center of the FTE, where the magnetic field lines are rolled up, the curvature effects should make the discontinuity more complex than a planar discontinuity. Also, in the case of a nonplanar discontinuity, the mass flux conservation should be considered by taking into account the possibility of fluxes along the magnetic field coming from the ionosphere as the Da discontinuity, located in between D1 and D2, is detected within the region of closed magnetic field lines. Thus, either the calculation of the normal velocities are not correct due to the curvature effects and Da could be a curved TD or the normal velocities are correct but the discontinuity analysis needs to include fluxes along the magnetic field lines and a more complex geometry in order that the mass flux be conserved. Considering that both options are speculative, we prefer to let the nature of Da, the discontinuity close to the center of the FTE, as being undetermined. D2 has a finite $\langle B_n \rangle$, a small $\langle \theta \rangle \sim 8^\circ$, smaller than the standard deviation (12°5). The tangential velocity jump at D2 is calculated from a formula obtained

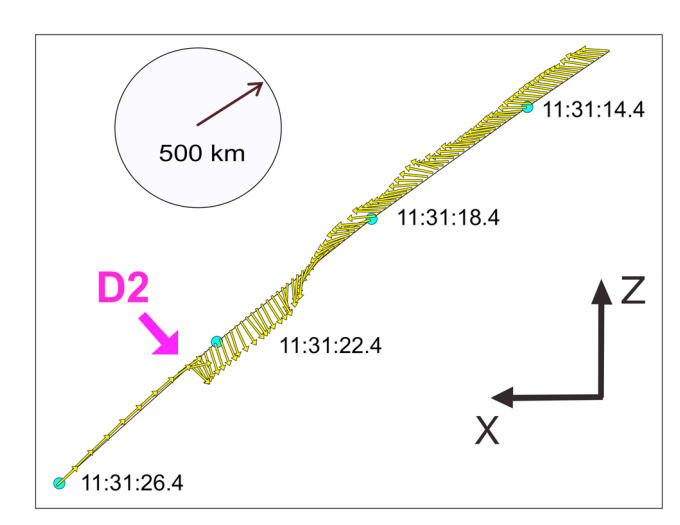


Figure 6. Zoom of the magnetic field components B_x and B_z taken around D2. The time interval between successive arrows is 0.3 s. The modulus of B is kept constant. Magnetic field vectors are plotted along a thin black line built by moving ions along the flow velocity vector measured every 4 s. At D2 the magnetic vector rotates in less than 1 s. The slower rotation observed before is due to the parallel current flowing in the core (see text).

by Hudson [1970]: $\delta \mathbf{V}_{\text{predicted}} = \mathbf{V}_{2t} - \mathbf{V}_{1t} = (1 - \alpha_1)^{1/2} (\mu_0 \rho_1)^{-1/2} [\mathbf{B}_{2t} (1 - \alpha_2) /$ $(1 - \alpha_1) - \mathbf{B}_{1t}$], where μ_0 is the magnetic permeability of vacuum, ϱ is the plasma mass density, $\alpha = (p_{\parallel} - p_{\perp})\mu_0/B^2$ describes the effect of the thermal anisotropy of ions, and p_{\parallel} and p_{\perp} are the parallel and perpendicular components to B of the plasma pressure. The velocity jump $\delta \mathbf{V}_t$ calculated from the above formula for D2 (\sim 180 km/s, the α parameter being computed from Composition distribution function (CODIF) temperature measurement, not shown and available at the Cluster Science archive) is larger than what is measured, namely, 71 km/s. A discussion and a possible explanation are given in Appendix B. The density slightly changes across D2 (Figure 3g). Figure 4j demonstrates that the ion flow is crossing D2; the normal component of the ion flow is conserved (~188 km/s before and 194 km/s after), as expected for a RD. In view of the

previous discussion we tentatively conclude that D2 is a RD. D3 also has a finite $\langle B_n \rangle$, $\langle \theta \rangle$ is small $(\sim 16^{\circ})$, smaller than the standard deviation $(\sim 21^{\circ})$ and the density variation is negligible. The normal velocity is approximately conserved. The jump of the tangential component calculated from Hudson's formula (148 km/s) matches the measured jump (149 km/s). D3 is interpreted as a RD.

4. Modeling

4.1. Magnetic Structures of D2 and D3

Figure 5 shows the magnetic field components B_{ν} and $B_{\tau i}$ in GSE (Figure 5a). This frame is chosen because it allows a decoupling between rapidly varying and slowly varying magnetic field components. At D2 B2 changes from -15 to +15 nT in less than 1 s while B_x is small and changes more slowly and B_y remains large and almost constant at this time scale. Fast variations are also observed in the $(XZ)_{gse}$ plane at D3 while B_y remains almost constant over the time scale of B_x and B_z variations. This behavior is the signature of the crossing of current

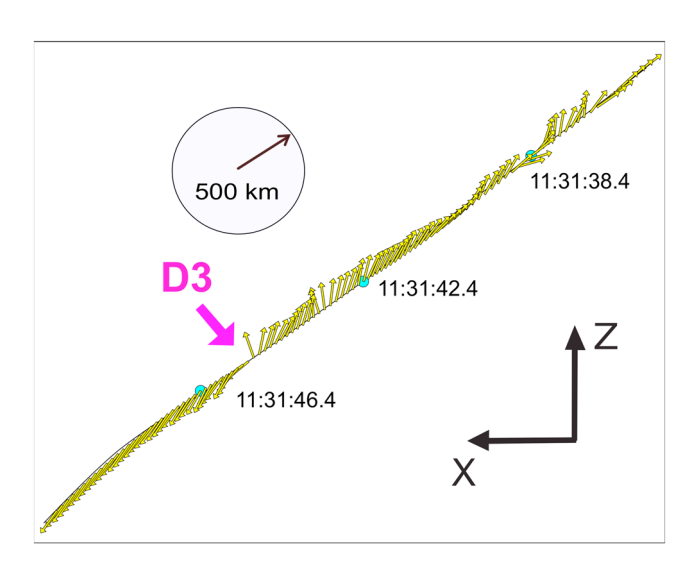


Figure 7. Same format as Figure 6 but taken at a later time, around D3. Notice the fast (<1 s) magnetic field rotation, by almost 180° Âr at D3.

sheets in the presence of a guide field (B_{ν}) . The thickness of this current sheet can be estimated from Figure 5b which is a zoom of the magnetic fields measured by the four spacecraft around D3; it shows that one by one the B_x and B_7 components cancel simultaneously on each spacecraft. The distance between spacecraft 4 and the others is about 600 km corresponding to a 6 s delay. On the other hand the field reversal at D3 takes about 1 or 2 s. Thus, the spacecraft cross a current sheet with a thickness of about 100-200 km; of the order of the ion Larmor radius. Figures 6 and 7 show again the magnetic field vectors projected on the (XZ) plane but it is now plotted along the ion flow trajectory. The ion flow trajectory is built by

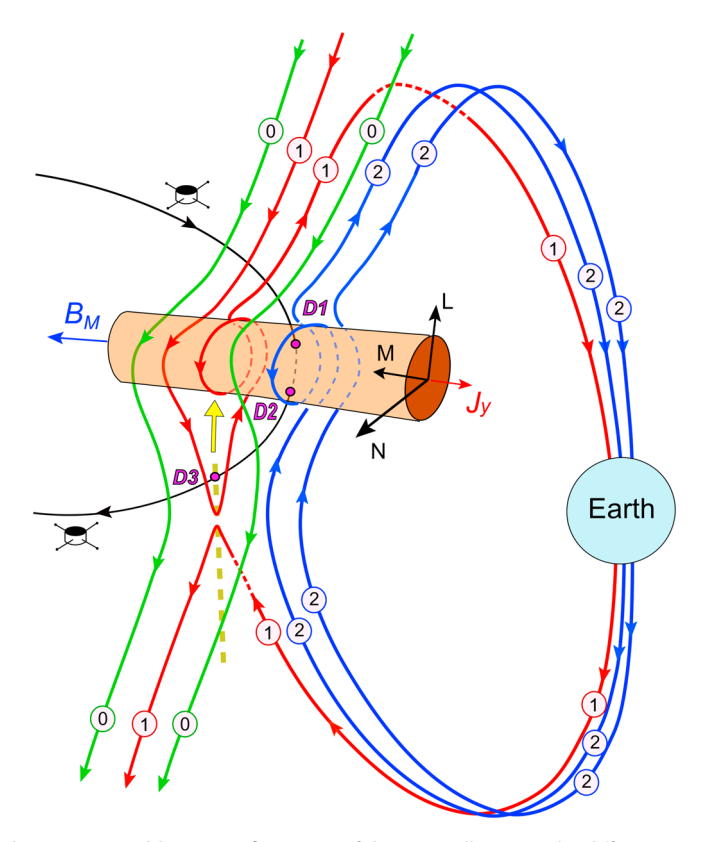


Figure 8. Schematic showing a possible 3-D configuration of the FTE. It illustrates the different types of field lines topologies and is consistent with the current density observed in the core. Circled numbers indicate the number of magnetic footprints on Earth.

moving the ion flow location by $V_i \cdot \Delta t$ at each step, where V_i is the ion bulk velocity and $\Delta t = 4$ s. High-resolution (0.3 s.) magnetic field data are zoomed around D2 (Figure 6) and D3 (Figure 7). The modulus of the magnetic field arrows is kept constant, to help visualize magnetic field rotation. D2 corresponds to the fast rotation (over less than 1 s) observed in Figure 6, around 1131:23 UT, on C2 and a few second later on other spacecraft. The slower anticlockwise rotation of magnetic vectors observed on C2 before crossing D2 is the signature of the parallel current characterized in section 2.3. D3 corresponds to the rapid rotation in the direction of the magnetic field observed in Figure 7, at about 1131:45 UT. The single arrow in the middle of the signature of D3 can be disregarded because it has a very small amplitude. Figures 6 and 7 help visualize the behavior of the magnetic field near the critical regions (D2 and D3); they will be used to build the model displayed in Figure 8.

4.2. Evolution of the Ion Jet

Figure 4b shows that the ion flow is accelerated through D3; the tangential component increases by almost a factor 2. The jump in the tangential magnetic field (~30 nT) and the jump in the tangential velocity (~149 km/s) satisfy the classical relation obtained by *Hudson* [1970] and already quoted above in section 3.4. Magnetosheath ions penetrate the FTE, through D3, in region C which corresponds to open field lines (see section 2). The normal component of the ion velocity is approximately conserved (~69 km s⁻¹ before and 81 km s⁻¹ after) and comparable to the projection of the de HT velocity along the normal (\sim 76 km s⁻¹). The motion of the discontinuity is slightly slower (65 km s⁻¹). This penetration occurs through the trailing edge of the FTE. Afterward accelerated magnetosheath ions penetrate through D2 on closed field lines; indeed, (i) the normal component of the flow velocity calculated by discontinuity analysis is approximately conserved (188 km s⁻¹ before and 194 km s⁻¹ after) and is close to the normal component of the de HT velocity, 196 km s⁻¹, and (ii) He⁺⁺ ions, from the solar wind, are observed between D2 and Da (not shown), on closed field lines. He⁺⁺ ions have bulk energies about 4 times that of H⁺ ions. The estimated velocity of the discontinuity (225 km s⁻¹) is consistent with the velocity of the ion flow at D3: 196 ± 56 km s⁻¹. Yet Table 1 indicates that the uncertainty in the estimate of the velocity of the discontinuity (56 km s⁻¹) is particularly large for

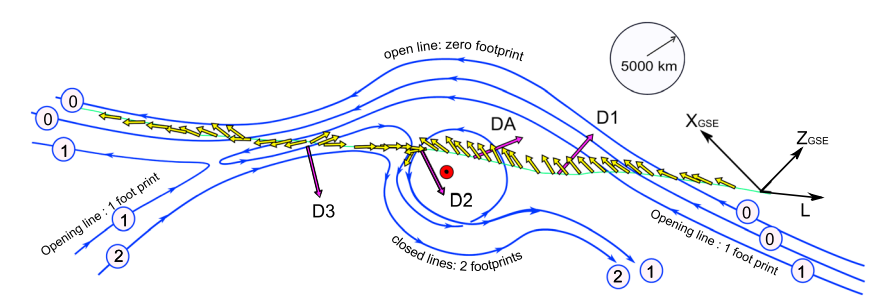


Figure 9. Schematic showing a possible magnetic configuration of the FTE, represented according to a 2-D perspective. This representation aims at showing the agreement between the observed magnetic field displayed as yellow arrows and the model. These arrows correspond to the modulus of the projection of the magnetic vector on the (XZ)_{ase} plane.

D2. We therefore conclude that, for D2, the two normal velocities have the same order of magnitude. On the other hand, for D2, the value of ΔV_t calculated from ΔB_t is almost 3 times larger than the measured one. As shown by Dunlop and Woodward [1998], curvature effects can also play a key role in the determination of the ratio between ΔV_t and ΔB_t . D2 being located at the boundary of a flux rope, curvature effects are indeed expected to be important and are likely to account for the ratio difference between ΔV_r calculated from ΔB_r and the observed value of ΔV_r . While accelerated ions continue to move poleward the flow velocity undergoes a large decrease at Da. At Da the normal component of the ion flow decreases from 215 km s⁻¹ to 154 km s⁻¹ and keeps on decreasing till the modulus reaches \sim 172 km s $^{-1}$ at D1 where it matches the magnetosheath velocity. This matching suggests that the FTE which moves faster than its front might undergo some kind of steepening or even breaking. Another evidence for steepening will be given in subsection 4.4.

4.3. Tentative Model

The proposed model is based on the preceding results summarized below: (i) FTEs can be divided in different regions: leading and trailing regions, (regions B and C), embedded in the magnetosheath and separated by smaller-scale discontinuities (D1, D2, and D3); (ii) magnetosheath ions penetrate through the trailing edge of the FTE where they are accelerated in a thin current sheet (D3); (iii) these ions penetrate in the core of the FTE on closed field lines connected to the Earth; and (iv) this leading region (core) corresponds to a large quasi-parallel current flowing azimuthally (along B_M). This current produces a helical magnetic field that plays a major role in determining the magneticfield in region B (between D1 and D2).

Given these constraints a model is sketched in Figure 8. D3 corresponds to the crossing of a thin current sheet where magnetosheath field lines merge with terrestrial field lines, which leads to ions jetting toward the core. D2 is at the boundary between open and closed field lines; between D2 and D1 field lines have two footprints on Earth. D2 is located where the current of the flux rope begins to play a major role at determining the geometry of magnetic field lines, as illustrated by Figure 8. The flux rope is "pushed" by poleward moving jetting ions (along L). The large antiparallel current between D1 and D2 produces helical magnetic field lines that make number of turns before joining the Earth. This current is likely carried by low-energy electrons. The electron anisotropies, shown in Figure 13 just before D2 crossing, have larger electron fluxes in parallel directions in the 36-50 eV energy range and would be consistent with this assumption. However, rapid variations of the magnetic field in the time scale of the spin period make particle measurements difficult to be interpreted at this time scale, and furthermore, the current carrier electrons could be even at lower energy below the lowest-PEACE energy range. The definitive identification of the nature of the current should be addressed by the instrument suite of the Magnetospheric multiscale (MMS) mission [Burch et al., 2015]. At D1 the velocity of the FTE front matches magnetosheath velocity. A different perspective is shown in Figure 9 which corresponds essentially to a projection, on the (XZ) plane, of Figure 8. The measured magnetic field arrows, plotted along the ion flow trajectory, are superimposed on the proposed magnetic configuration. Figure 9 illustrates the matching between the model and the directions of measured magnetic vectors. In the model displayed in Figure 9, the reversal of the L component observed at D3 corresponds to a slight upward (in the Z direction) displacement of D3 with respect to the spacecraft, while D2 corresponds to the transition between field lines having one and two magnetic footprints on Earth. The number of footprints on Earth is indicated by a circled number.

4.4. Temporal Evolution of the FTE

The locations of the discontinuities, the direction of their normal vectors and the orientation of the magnetic field are used to build the shape of the FTE projected on the (XZ) plane and its time evolution on Figure 10.

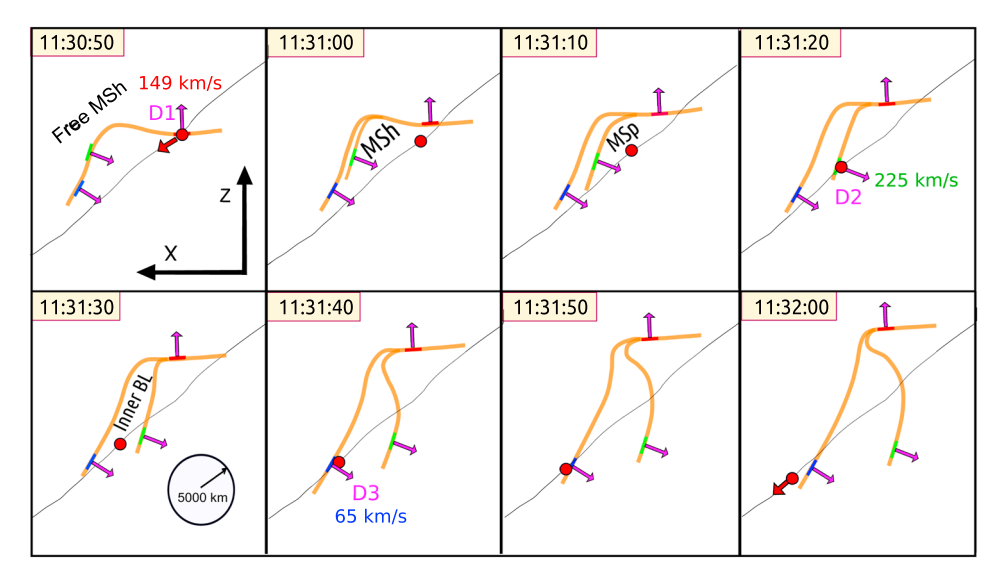


Figure 10. Composite view showing the projection, on the $(XZ)_{gse}$ plane, of the shape of the FTE at successive times; one panel every 10 s. The evolution of the shape is built by extrapolating the motion of the discontinuities: D1 (red), D2 (green), and D3 (blue). The thin black line is drawn along the ion flow velocity measured on board at C1 location. Red dots show where C1 was at the time indicated on each panel. (first panel) Discontinuities D2 and D3 merge when D1 is crossed by the satellite. (last panel) The profile of the FTE breaks around 1132 UT; see text.

In Figure 10 the successive positions of the spacecraft are indicated by red dots. The panels are equally spaced in time; one every 10 s. The structure of the FTE shown in Figure 10 looks like a poleward moving bump protruding first outward and then inward, similar to the one described by Sibeck [1990]. Yet at variance with Sibeck's model the trailing edge of the bump splits into two RDs and the magnetosheath plasma penetrates through these discontinuities. D2 and D3 are found to move at different normal velocities; D3 moves at \sim 65(\pm 7) km s⁻¹, while D2 is moving at \sim 225(\pm 56) km s⁻¹. Under the assumption that the discontinuities move along their normal vectors at constant velocities, the position of each of the discontinuities and the corresponding temporal evolution of the FTE are calculated at earlier times. This backward extrapolation indicates that the discontinuities D2 and D3 did coincide (were stacked together or superposed) around 1130:50 (see Figure 10 (first panel)) when the spacecraft crossed D1. This coincidence/stacking is to be expected since D2 and D3 are almost parallel and D3, the last to be met, moves slower than D2. Thus, given that D2 and D3 carry currents in opposite directions their colocation could correspond to a weak local parallel current. Yet this signature could also be associated with the crossing of a separatrix. This interpretation implies that the splitting, and presumably the ion jet acceleration, started after 1130:50 which tell us that the splitting occurred less than 2 R_F (40 s times 300 km s⁻¹) below the spacecraft; that is around $Z \sim 7$ R_F which is well off equator. Event 2 is a case of stacked configuration; it is discussed in section 6. The FTE could also have been initiated nearer from the equator, as a magnetic vortex, but with no magnetosheath plasma penetration. On the other hand the forward extrapolation (Figure 10) indicates that about 30 s later the FTE bulge steepens and tends to break, as time evolves, which confirms an earlier suggestion (section 4.3). Thus, it seems that the lifetime of the FTE might be shorter than expected or that the FTE is not continuously evolving. The examination of event 2 (in section 6) will fuel this discussion. Before this we will look for a process that could break down the frozen in of the plasma and allow the acceleration and penetration of magnetosheath plasma inside the FTE.

5. Electron Acceleration

Figure 11 shows the flux of low-energy (\sim 36 eV to \sim 200 eV) electrons versus pitch angle, in three energy ranges. As expected electrons in the lowest energy range have large fluxes in the magnetosheath, outside the FTE, in regions A and D. Inside the FTE large fluxes of bidirectional electrons are observed in the three energy ranges but not during the same time periods. In the lowest energy channel (36–50 eV) large fluxes of bidirectional electrons are observed between D2 and D3 (region C), but their flux is particularly small between D1 and Da, which corresponds to the density depletion shown in Figure 4a and to the region where accelerated ions do not penetrate as described in subsection 4.1. At slightly higher energies (50–100 eV) enhanced fluxes of electrons are also observed in the parallel and antiparallel directions, between Da and D3 and hence on

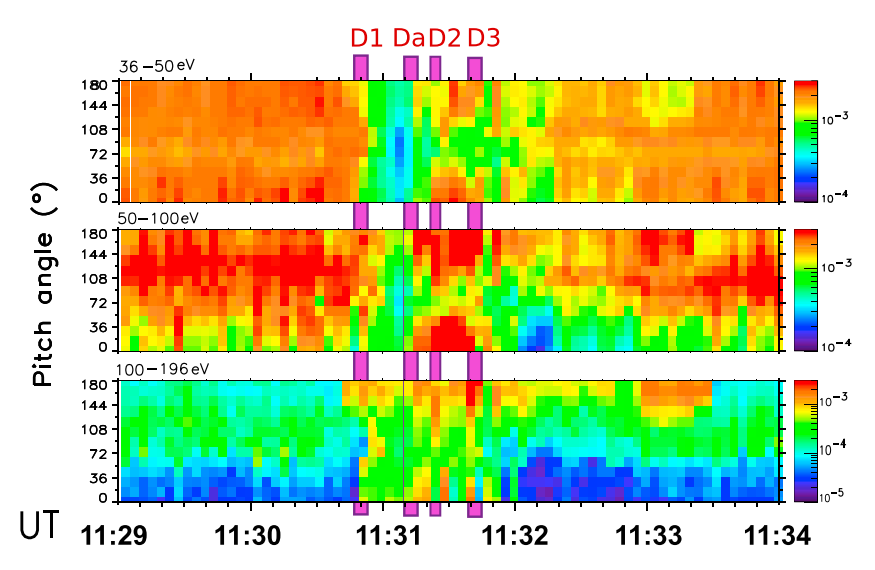


Figure 11. Angular distribution of the flux (in erg/cm² s str eV) of low-energy electrons in three energy ranges: (top) 36–50 eV, (middle) 50–100, (bottom) 100–196. Discontinuities are indicated by violet spots. Bidirectional field-aligned electrons are observed inside the FTE over time periods that depend upon the energy channel.

open as well as on closed field lines. At still higher energies (100–200 eV) the electron flux is more sporadic but remains generally bidirectional and covers the whole time interval between D1 and D3. In the three cases the fluxes are comparable or larger than in the magnetosheath, indicating that the observed electrons come from the magnetosheath and are accelerated or heated in the parallel and antiparallel directions. These bidirectional fluxes of electrons can play an important role at breaking the frozen-in approximation; it is therefore interesting to try to understand how they are formed. Two possible mechanisms are considered: wave acceleration/heating and DC E-Field.

5.1. Wave Acceleration/Heating

As already mentioned, wave intensity is strongly enhanced, in particular between 1131:10 (Da) and 1131:45 (D3). This time interval corresponds to the bidirectional accelerated electrons, shown in Figure 11 (middle), suggesting a possible link between waves and electron heating/acceleration. Chaston et al. [2008, 2012] and Roux et al. [2011] made similar observations on the basis of Cluster and THEMIS data. They showed that the waves they observed near the magnetopause were kinetic Alfvén waves (KAWs) with large $k_{\perp}\rho_{i}$. Their frequencies in the spacecraft frame are strongly Doppler shifted and largely exceed the frequency in the plasma frame.Given that KAWs have a small but finite δE_{\parallel} they can heat electrons along field lines, in parallel and antiparallel directions via inverse Landau damping. The wave parallel electric field can break the frozen-in condition and the amplitude of waves (\sim 3 nT) is large and could therefore ensure the transport of ions. In this interpretation, however, heated/accelerated electrons should have $V_{\parallel,e} \sim \omega/k_{\parallel}$ with $\omega = \pm k_{\parallel}V_Ak_{\perp}\rho_i/\sqrt{\beta_i + 2/(1 + T_e/T_i)}$ given by the KAW dispersion relation (β_i being the ratio between the ion thermal pressure and the magnetic pressure, and T_i (respectively, T_e) being the ion (respectively, electron) temperature) [see, for instance, Sahraoui et al., 2009, and references therein]. Given that V_A , the Aflvén velocity $(B/\sqrt{\mu_0 m_i n_i})$, is relatively small (~150 km s⁻¹) large $k_{\perp}\rho_i$ are needed to fulfill the above condition. Thus, wave heating is a viable process for the lowest-energy channels but probably not for the 100-200 eV; another explanation is proposed in the next section.

5.2. DC E Fields

The energy versus time dependence of bidirectional electrons observed in Figure 11 can be produced by a parallel electric potential localized inside the FTE with a maximum near D1 (so mostly on closed field lines) and decreasing between D1 and D3. Thus, the initially very low energy magnetosheath electrons that penetrate the FTE gain a parallel energy that depends on how deep they get in; that is how close from D1. Between D3 and D2, they gain \sim 40 eV, while further inside, between D2 and Da and hence on closed field lines they gain \sim 100 eV. In this model electrons are accelerated and trapped along the guide field (parallel and antiparallel) which is essentially in the azimuthal direction. The presence of a parallel electric potential can be understood as a consequence of quasi-neutrality. Electrons have a much higher mobility than ions, therefore when

15

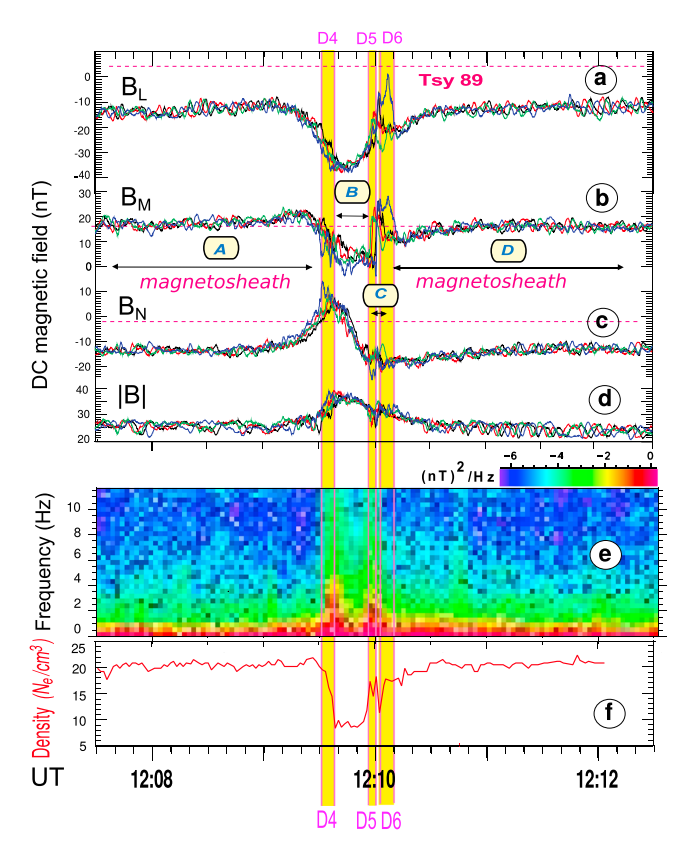


Figure 12. Zoom on FTE period. Similar to Figure 3 but concerns event 2. The three discontinuities D4, D5, and D6 separating different regions of space are shown in yellow.

charged particles penetrate in the FTE, electrons tend to move away from the FTE faster than ions along field lines. Thus quasi-neutrality implies the existence of a parallel electric field to preserve charge neutrality inside the FTE [see *Le Contel et al.*, 2000]. Such a parallel electric field could be also due to the electron pressure gradient term in the generalized Ohm law as the spatial scale of the discontinuities reaches the electron scale [see, for instance, *Henderson et al.*, 2008]. In the present case a maximum in the parallel potential can trap low-energy electrons and accelerate them along the magnetic field in parallel and antiparallel directions, as is observed. The potential also regulates the entry of ions. Given that ions have been accelerated through D3, most ions can penetrate in the core as long as their energy exceeds that of the potential barrier: $\sim 50-100$ eV, which explains why ion, accelerated through D3 hardly cross Da. Note that quasi-neutrality also implies the presence of parallel currents [*Le Contel et al.*, 2001]; we have indeed given evidence for a large parallel current localized between D1 and D2 (in section 2.3 and Figure 3e). The structure of this current is sketched in Figure 8.

6. Analysis of Event 2

6.1. Fields and Currents

Figures 12a–12d show full-resolution data from FGM, in boundary normal coordinates, obtained from MVA applied to the period covered by Figure 2. For this event, the Cluster location in GSE is approximately (9.2, 8.65, and 6.3, see also Figure 1). Again, we see the typical signature of a FTE, with a bimodal signature (\pm) on B_N , and an increase in the modulus of $\bf B$, from 25 nT to 40 nT, around 1209:40. As for event 1 this maximum occurs during the early phase of the event; large-amplitude variations in the L direction occur later. As for event 1 narrow vertical yellow regions, bracketed by pink lines, outline the fast variations in the magnetic field and/or the density; they are referred to as D4 (\sim 1209:35), D5 (\sim 1209:55), and D6 (\sim 1210:05). The density estimated from Waves of high frequency and sounder for probing of electron density by relaxation (WHISPER) the relaxation sounder [*Décréau et al.*, 1997] is shown in panel Figure 12f. Before crossing D4 and after crossing D6 the density is \sim 20 p cm⁻³, as expected for the magnetosheath. Between D4 and D5 a large-density drop is observed, together with an increase in the modulus of $\bf B$, and a classical bipolar signature of B_N . The dynamical

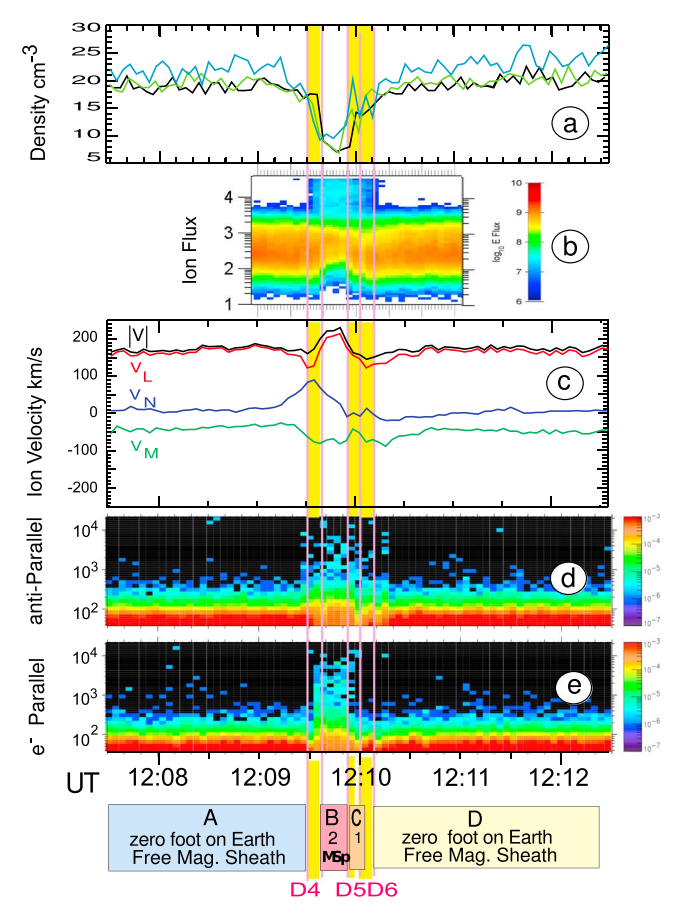


Figure 13. Particle data for event 2. The format is similar to Figure 4. Notice the large-density drop between D4 and D5.

spectrum of magnetic fluctuations displayed in Figure 12e, gives evidence for magnetic fluctuations with an extended frequency bandwidth and enhanced amplitudes at the boundaries of the FTE (at D4 and D5). Yet the amplitude \sim 0.2 nT is more than 10 times smaller than for the first event.

6.2. lons

Figures 13a–13c show ion data, in GSE. The ion density displayed in Figure 13a is consistent with relaxation sounder data (Figure 12f). Figure 13b shows the ion flux versus energy and time. In regions A (before 1209:30) and D (after 1210:10) the spacecraft measure a low-energy relatively dense (\sim 20 p cm⁻³) plasma typical of the magnetosheath. Energetic ions are detected between 1209:30 and 1210:10 (periods B and C), while the FTE is crossed. Unlike event 1 escaping energetic ions and electrons (see Figures 13b and 13d) do not continue to be observed after the magnetic signature of the FTE. The flow velocity component is $V_L \sim -170 \text{ km s}^{-1}$ in the free magnetosheath (regions A and D). Its modulus is slightly enhanced during the FTE and reaches $V_L \sim -220 \text{ km s}^{-1}$ in region B.

6.3. Electrons

Figure 13 shows the electron flux, in directions antiparallel (d) and parallel (e) to $\bf B$ for C3. There are almost no electrons beyond a few hundred eV in regions A (before 1209:30) and D (after 1210:10) which confirms that regions A and D correspond to the free magnetosheath, with no magnetic footprint on Earth. A sudden increase in the electron flux above 1 keV is observed at \sim 1209:30 in the antiparallel flux (Figure 13d), in the perpendicular flux (not shown) and slightly later (one or two spin period later) in the parallel one (Figure 13e), while the magnetic signature of the FTE develops. A similar behavior is observed on other spacecraft. Being farther C1 observes energetic parallel electrons during a shorter time period while C4 which is closer observes energetic electrons during a longer time period. As for event 1 the flux of energetic electrons above 1 keV in region B (see Figures 13d and 13e) does not change much with pitch angle, which is typical of closed field lines.



Table 2. Similar to Table 1 but for Event 2 ^a						
	D4	D5	D6			
n _x	0.35	-0.90	- 0.80			
n_y	0.49	-0.44	-0.48			
n_z	0.80	-0.05	-0.36			
$\Delta \alpha$ (°)	10	12.5	4.5			
θ (°)	27	66.5	10.5			
$\Delta heta$	13	30	12			
$< B_n > (nT)$	-2.5	0.04	7			
Δho (p cm $^{-3}$)	-10	- 7	~ 0			
Summary	large θ	large θ	small $ heta$			
	large Δho	large Δho	small Δho			
		small $< B_n >$	$large < B_n >$			
Nature	TD	TD	RD			
^a Conclusion line in boldface.						

Hence, region B corresponds to closed field lines. Thus, in the leading region of the FTE (region B), field lines are closed. Large fluxes of antiparallel energetic electrons (escaping from the magnetosphere) continue to be observed in region C, but the parallel fluxes of energetic electrons get very small, from 1209:55 to 1210:10 (see Figure 13e). Region C corresponds to open field lines connecting the magnetosphere to the magnetosheath. The two discontinuities D5 and D6 are nearby and region C is small.

6.4. Discontinuity Analysis

Table 2 shows the outcome of discontinuity analysis for event 2. The format is about the same as for Table 1. For event 2, however, we did not identify a discontinuity corresponding to Da. Table 2 shows that for D4, $< B_n >$ is

17

finite, but θ is larger than the standard deviation, and ΔN is large; we therefore conclude that D4 is a TD. D5 has a very small $< B_n >$, a large θ , and a large ΔN ; it is a TD. D6 has a large B_n , a small θ , and a negligible density variation; it is a RD. D5 and D6 being too close we could not carry out a reliable de HT analysis of individual discontinuities for event 2.

6.5. Comparison Between the Two Events

While event 2 is shorter, it shares many characteristics with event 1. For both events region B is characterized by (i) nearly isotopic energetic electrons, (ii) a strong density depletion, and (iii) a maximum in the modulus of B. Hence, for both events region B is on closed field lines. In region C (i) energetic electrons are still present but they are strongly anisotropic and escape along open field lines and (ii) the density is close to that of the magnetosheath. As for event 1 region C corresponds to field lines connecting the Earth to the magnetosheath (one foot on Earth). For event 2, however, D5 and D6 are stacked together and we do not observe a penetration of the magnetosheath plasma, nor do we observe any evidence for enhanced fluxes of bidirectional low-energy electrons. The event 2 FTE is no longer injecting magnetosheath plasma on closed magnetospheric field lines. Thus, it seems that FTEs can be either active or passive.

7. Summary and Conclusions

A multipoint and multi-instrument study of two FTEs has led to the following results.

- 1. The two FTEs can be divided in different regions: the leading and the trailing regions separated by sharp discontinuities associated with thin current sheets.
- 2. Remote sensing of field line topology, via energetic electrons, and estimates of electron temperature lead to conclude that magnetic field lines in the leading region are closed, with two footprints on Earth, while field lines in the trailing region are opened, with one footprint on Earth. Possible configurations of closed and opened field lines are shown in Figures 8 and 9.
- 3. Field lines in the leading region (region B) form a flux rope oriented essentially in the azimuthal direction. The corresponding current ($\sim 25 \text{ nA/m}^2$) produces a helical magnetic field which is stronger than the dipole field and opposed to it.
- 4. For event 1 magnetosheath ions penetrate through the edge of the trailing region (region C) of the FTE where they are accelerated in a thin current sheet (D3) corresponding to a rotational discontinuity. Then accelerated ions penetrate through D2 (also a RD) in region B, on closed field lines, at least for event 1, but for the second event few magnetosheath ions and electrons penetrate in the flux rope because they can hardly cross D5 (apart from finite Larmor radii effects) which is a TD. We therefore conclude that event 1 corresponds to an active FTE injecting magnetosheath plasma in the magnetosphere, while event 2 is passive; presumably the remnant of an active FTE. In what follows we concentrate on event 1.
- 5. The orientations of the discontinuities and the directions of the magnetic field were used to determine the shape of the FTE. The FTE looks like a bump protruding first outward and then inward. It moves poleward



- (more precisely along L). This is similar to the model proposed by Sibeck [1990]. Yet at variance with Sibeck's model the trailing edge of the FTE splits in two rotational discontinuities that accelerate magnetosheath ions and inject them on closed field lines.
- 6. The determination of the velocity of the discontinuities D2 and D3 along their normal vectors allows an estimate of their locations at earlier times, assuming that discontinuities move at constant velocities and directions. This backtracking (back in time) leads to conclude that about 40 s (corresponding to $\sim 2 R_F$) before being crossed by the spacecraft the two discontinuities were colocated or stacked together. Given that they correspond to oppositely directed currents, the sum produces a very small total current which suggests that current sheet acceleration was not yet active in the stacked configuration. For event 2 the stacked configuration was not found to drive the penetration of the magnetosheath plasma. The FTE could have started nearer from the equator, as a magnetic vortex with no interpenetration of surrounding plasmas. Magnetic activity might also be periodic.
- 7. On the other hand when D2 and D3 are moved forward to infer the evolution at later times, the FTE is found to steepen and possibly break. This might suggest some kind of periodic formation/breaking that brings together topologically distinct domains, like in the simulations of Dorelli and Bhattacharjee [2009].
- 8. The energy/time signatures of the observed bidirectional (parallel and antiparallel) low-energy electrons, within the FTE, are tentatively interpreted in terms of a positive parallel electric potential, localized inside the FTE, that traps magnetosheath electrons and prevents them from leaving too rapidly the FTE. The deeper electrons penetrate in the FTE (i.e., the closer from the leading edge), the larger their energy gain. Hence, the presence of an electric potential can be driven by the need to preserve charge neutrality. This parallel electric field breaks the frozen-in condition.
- 9. Event 2 shares many characteristics with event 1. Yet unlike event 1 the two discontinuities observed at the trailing edge of event 2 are stacked together and do not allow the transport on closed field lines. The comparison between the two events as well as the inferred evolution of D2 and D3 (see point 6) suggests that FTEs could exist in two states depending on whether current sheets located at the trailing edge are split or stacked. In split current sheets the acceleration of magnetosheath ions and their penetration on closed field lines occur at different places; reconnection is "active." In stacked current sheets the magnetosheath plasma can be accelerated, but it does not penetrate on closed field lines. More events should be analyzed before transforming this suggestion into a firm conclusion.

Appendix A: Uncertainty on θ

The uncertainty in the determination of θ comes from two sources (i) the uncertainty in the knowledge of the directions of ΔV and ΔB and (ii) the uncertainty associated with their projections on the discontinuity. The latter is due to the uncertainty in the determination of the direction of the normal **n**. This uncertainty, $\Delta \alpha$, is given in Table 1; it can reach 18°. It is easy to see, however, that this uncertainty, which intervenes in the projection of an angle, provides a second-order contribution to θ ; hence, it has a small influence on the results. To show this, let τ be the measured angle between ΔV_t and ΔB_t ; τ is related to θ via the classical formula:

$$\cos(\tau) = \cos(\theta)\cos(\gamma)\cos(\omega) + \sin(\gamma)\sin(\omega) \tag{A1}$$

where γ and ω are the angles between ΔV and ΔB and the plane of the discontinuity. We assume that $\gamma \sim \omega$ are small and notice that they are of the order of the standard deviation $\Delta \alpha$. Then, expanding the trigonometric functions in the small parameter $\Delta \alpha$ we find from (A1)

$$\cos(\tau) = \cos(\theta + \delta\theta) \sim \cos(\theta) - \delta\theta \sin(\theta) \sim \cos(\theta) [1 - \Delta\alpha^2] + \Delta\alpha^2$$
 (A2)

After simplification, we get from (A2)

$$\delta\theta = (\Delta\alpha)^2(\cos\theta - 1)/\sin\theta \sim (\Delta\alpha)^2(\theta/2) \tag{A3}$$

for small θ .



 $\Delta \alpha$ and θ are given in Table 1. (A3) shows that the uncertainty on α gives only a small contribution to the error on θ : ~ 4° for D1, 0.4° for D2, 0.12° for D3, 0.4° for D4, 1.8° for D5, and 0.04° for D6.

Regarding the other error source we estimate that the uncertainty in the determination of the direction of ΔV_{\star} is of the order of 10%. **B** is known within an accuracy better than 0.1 nT. Thus, for the sake of simplification we neglect the uncertainty on B. Thus, θ is defined by

$$\sin \theta = (\Delta \mathbf{V} \times \Delta \mathbf{B}) / (\Delta V \Delta B) \tag{A4}$$

Where the indexes have been dropped. After some straightforward algebra we get to the lowest order

$$\delta\theta \sim [\delta(\Delta V)/(\Delta V)][(\sin(\theta) - 1)]/(\cos\theta)$$
 (A5)

$$\delta\theta < 2[\delta(\Delta V)/(\Delta V)]/(\cos\theta)$$
 (A6)

Assuming $[\delta(\Delta V)]/(\Delta V) \sim 0.1$, we find $\delta\theta < 0.2/(\cos\theta)$. This formula is used in Tables 1 and 2.

Appendix B: Uncertainty on δV_r

According to Khrabrov and Sonnerup [1998] and Dunlop and Woodward [1998], there are at least two reasons that could explain the difference between the two estimates of δV_r : (i) the motion of the discontinuity could be nonuniform and (ii) the discontinuity could be nonplanar. The first option is unlikely because the normal components of the ion velocity measured on both sides of D2 are about the same. The second possibility is more likely to explain the difference because D2 has been shown to correspond to a flux rope and hence should have a more or less circular cross section, as illustrated in Figure 8. An independent argument is given below. For each spacecraft we have calculated the normal **n** to D2 by minimum variance analysis. Then the divergence of \mathbf{n} gives the scale of the curvature: \sim 3800 km which corresponds approximately to the size of the flux tube (10 s times 370 km/s). Thus, the curvature of the discontinuity is likely to explain the difference between the predicted and the measured values of δV_t .

Acknowledgments

We are grateful to Gérard Chanteur who kindly provided us with the software for calculating normal vectors to discontinuities. The French participation to Cluster was funded by CNES, CNRS, and ESA. The data used in this paper are available at Cluster Science Archive (http://http://www.cosmos.esa.int/web/csa).

Larry Kepko thanks the reviewers for their assistance in evaluating this paper.

References

Balogh, A., et al. (1997), The Cluster magnetic field investigation, Space Sci. Rev., 79, 65-91.

Berchem, J., and C. Russell (1984), Flux transfer events on the magnetopause: Spatial distribution and controlling factors, J. Geophys. Res.,

Bosqued, J. M., et al. (2001), Cluster observations of the high-latitude magnetopause and cusp: Initial results from the CIS ion instruments, Ann. Geophys., 19, 1545 – 1566, doi:10.5194/angeo-19-1545-2001.

Burch, J. L., T. E. Moore, R. B. Torbert, and B. L. Giles (2015), Magnetospheric multiscale overview and science objectives, Space Sci. Rev., doi:10.1007/s11214-015-0164-9.

Chanteur, G. (1998), Spatial interpolation fo four spacecraft: Theory, in Analysis Methods for Multi-Spacecraft Data, ISSI Sci. Rep. SR-001, edited by G. Paschman and P. Daly, chap. 14, pp. 349-369, Eur. Space Agency, Noordwijk, Netherlands.

Chanteur, G., and C. Harvey (1998), Spatial interpolation fo four spacecraft: Application to magnetic gradients, in Analysis Methods for Multi-Spacecraft Data, ISSI Sci. Rep. SR-001, edited by G. Paschman and P. Daly, chap. 15, pp. 371 – 393, Eur. Space Agency, Noordwijk, Netherlands.

Chaston, C., et al. (2008), Turbulent heating and cross-field transport near the magnetopause from THEMIS, Geophys. Res. Lett., 35, L17S08, doi:10.1029/2008GL033601.

Chaston, C. C., J. W. Bonnell, L. Clausen, and V. Angelopoulos (2012), Energy transport by kinetic-scale electromagnetic waves in fast plasma sheet flows, J. Geophys. Res., 117, A09202, doi:10.1029/2012JA017863.

Cornilleau-Wehrlin, N., et al. (1997), The Cluster Spatio-temporal Analysis of Field Fluctuations (STAFF) experiment, Space Sci. Rev., 79, 107-136.

Décréau, P., et al. (1997), WHISPER, a resonance sounder and wave analyser: Performances and perspectives for the CLUSTER mission, Space Sci. Rev., 79, 157-193.

Dorelli, J. C., and A. Bhattacharjee (2009), On the generation and topology of flux transfer events, J. Geophys. Res., 114, A06213, doi:10.1029/2008JA013410.

Dunlop, M., and T. Woodward (1998), Multi-spacecraft discontinuity analysis: Orientation and motion, in Analysis Methods for Multi-Spacecraft Data, ISSI Sci. Rep. SR-001, edited by G. Paschman and P. Daly, chap. 11, pp. 271 – 305, Eur. Space Agency, Noordwijk, Netherlands.

Dunlop, M., A. Balogh, D. Southwood, R. C. Elphic, K.-H. Glassmeier, and F. M. Neubauer (1990), Configurational sensitivity of multipoint magnetic field measurements, in Proceedings of the International Workshop on "Space Plasma Physics Investigations by Cluster and Regatta", Graz, Feb. 20-22, 1990, ESA SP-306, edited by E. Rolfe, pp. 20-22, Eur. Space Agency, Paris, France.

Elphic, R. C. (1995), Observations of flux transfer events: A review, in Physics of the Magnetopause, Geophys. Monogr. Ser., vol. 90, edited by P. Song, B. U. Ö. Sonnerup, and M. F. Thomsen, pp. 225–233, AGU, Washington, D. C.

Fedder, J. A., S. P. Slinker, J. G. Lyon, and C. T. Russell (2002), Flux transfer events in global numerical simulations of the magnetosphere, J. Geophys. Res., 107(A5), 1048, doi:10.1029/2001JA000025.

DAGU Journal of Geophysical Research: Space Physics

- Gustafsson, G., et al. (1997), The electric field and wave experiment for the Cluster mission, Space Sci. Rev., 79, 137 156.
- Henderson, P. D., C. J. Owen, A. D. Lahiff, I. V. Alexeev, A. N. Fazakerley, L. Yin, A. P. Walsh, E. Lucek, and H. Rème (2008),
 - The relationship between j imes B and ∇ P_e in the magnetotail plasma sheet: Cluster observations, *J. Geophys. Res., 113*, A07S31, doi:10.1029/2007 JA012697
- Hudson, P. D. (1970), Discontinuities in an anisotropic plasma and their identification in the solar wind, Planet. Space Sci., 18, 1611 1622, doi:10.1016/0032-0633(70)90036-X.
- Johnstone, A., et al. (1997), PEACE: A plasma electron and current experiment, Space Sci. Rev., 79, 351 398.
- Khrabrov, A. V., and B. U. Ö. Sonnerup (1998), DeHoffmann-teller analysis, in Analysis Methods for Multi-spacecraft Data, ISSI Sci. Rep. Ser.-001, edited by G. Paschmann and P. Daly, pp. 221-248, Eur. Space Agency, Netherlands.
- Landau, L. D., and E. M. Lifshitz (1960), Electrodynamics of Continuous Media, Pergamon Press, Oxford, U. K.
- Le Contel, O., R. Pellat, and A. Roux (2000), Self-consistent quasi-static parallel electric field associated with substorm growth phase, J. Geophys. Res., 105, 12,945-12,954.
- Le Contel, O., S. Perraut, A. Roux, and R. Pellat (2001), Plasma transport during growth phase and relation to breakup during substorm growth phase, Space Sci. Rev., 95, 415-426.
- Marchaudon, A., J.-C. Cerisier, R. A. Greenwald, and G. J. Sofko (2004), Electrodynamics of a flux transfer event: Experimental test of the Southwood model, Geophys. Res. Lett., 31, L09809, doi:10.1029/2004GL019922.
- Mottez, F., and G. Chanteur (1994), Surface crossing by a group of satellites: A theoretical study, J. Geophys. Res., 99, 13,499-13,507, doi:10.1029/93JA03326.
- Øieroset, M., et al. (2011), Direct evidence for a three-dimensional magnetic flux rope flanked by two active magnetic reconnection X lines at Earth's magnetopause, Phys. Rev. Lett., 107(16), 165007, doi:10.1103/PhysRevLett.107.165007
- Owen, C. J., et al. (2001), Cluster PEACE observations of electrons during magnetospheric flux transfer events, Ann. Geophys., 19, 1509-1522, doi:10.5194/angeo-19-1509-2001.
- Paschmann, G., G. Haerendel, I. P. N. Sckopke, S. Bame, J. Gosling, and C. Russel (1982), Plasma and magnetic field characteristics of magnetic flux transfer events, J. Geophys. Res., 87, 2159-2168.
- Phan, T., et al. (2004), Cluster observations of continuous reconnection at the magnetopause under steady interplanetary magnetic field conditions, Ann. Geophys., 22, 2355-2367, doi:10.5194/angeo-22-2355-2004.
- Pu, Z. Y., J. Raeder, J. Zhong, Y. V. Bogdanova, M. Dunlop, C. J. Xiao, X. G. Wang, and A. Fazakerley (2013), Magnetic topologies of an in vivo FTE observed by Double Star/TC-1 at Earth's magnetopause, Geophys. Res. Lett., 40, 3502 - 3506, doi:10.1002/grl.50714.
- Raeder, J. (2006), Flux transfer events: 1. Generation mechanism for strong southward IMF, Ann. Geophys., 24, 381-392, doi:10.5194/angeo-24-381-2006.
- Rème, H., et al. (1997), The CLUSTER ion spectrometry experiment, Space Sci. Rev., 79, 303-350.
- Robert, P., M. Dunlop, A. Roux, and G. Chanteur (1998), Accuracy of current density determination, in Analysis Methods for Multi-Spacecraft Data, ISSI Sci. Rep. SR-001, edited by G. Paschman and P. Daly, chap. 16, pp. 395-418, Eur. Space Agency, Netherlands.
- Robert, P., O. Lecontel, A. Roux, P. Canu, D. Fontaine, G. Chanteur, J. M. Bosqued, C. Owen, A. N. Fazakerley, and M. W. Dunlop (2006), Study of a flux transfer event with Cluster spacecraft, in Cluster and Double Star Symposium, 5th Anniversity of Cluster in Space, Edited by K. Fletcher, ESA SP-598, Eur. Space Agency, Noordwijk, Netherlands.
- Roux, A., P. Robert, O. Le Contel, V. Angelopoulos, U. Auster, J. Bonnell, C. M. Cully, R. E. Ergun, and J. P. McFadden (2011), A mechanism for heating electrons in the magnetopause current layer and adjacent regions, Ann. Geophys., 29, 2305-2316, doi:10.5194/angeo-29-2305-2011.
- Russell, C., and R. Elphic (1979), ISEE observations of flux transfer events at the dayside magnetopause, Geophys. Res. Lett., 6, 33 36.
- Sahraoui, F., M. L. Goldstein, P. Robert, and Y. V. Khotyaintsev (2009), Evidence of a cascade and dissipation of solar-wind turbulence at the electron gyroscale, Phys. Rev. Lett., 102(23), 231102, doi:10.1103/PhysRevLett.102.231102.
- Saunders, M., C. Russel, and N. Skopke (1984), Flux transfer events: Scale size and interior structure, Geophys. Res. Lett., 11, 131-134.
- Schwartz, S. (1998). Shock and discontinuity normals. Mach numbers and related parameters, in Analysis Methods for Multi-Spacecraft Data. ISSI Sci. Rep. SR-001, edited by G. Paschman and P. Daly, chap. 10, pp. 249-270, Eur. Space Agency, Netherlands.
- Sibeck, D. G. (1990), A model for the transient magnetospheric response to sudden solar wind dynamic pressure variations, J. Geophys. Res., 95, 3755-3771, doi:10.1029/JA095iA04p03755.
- Sonnerup, B. Ö., I. Papamastorakis, G. Paschmann, and H. Lühr (1987), Magnetopause properties from AMPTE/IRM observations of the convection electric field: Method development, J. Geophys. Res., 92, 12,137 – 12,159.
- Tan, B., Y. Lin, J. D. Perez, and X. Y. Wang (2011), Global-scale hybrid simulation of dayside magnetic reconnection under southward IMF: Structure and evolution of reconnection, J. Geophys. Res., 116, A02206, doi:10.1029/2010JA015580.
- Tsyganenko, N. A. (1987), Global quantitative models of the geomagnetic field in the cislunar magnetosphere for different disturbance levels, Planet Space Sci., 35, 1347 - 1359.